

## Article

# Design of Reflective Tunable Structural Color Metasurface Based on Guided-Mode Resonance Filter and $\text{Sb}_2\text{S}_3$

Shishang Luo, Zhenfu Zhang, Xin He , Zhaojian Zhang , Xin Li, Meicheng Fu  and Junbo Yang \*

College of Science, National University of Defense Technology, Changsha 410073, China

\* Correspondence: yangjunbo@nudt.edu.cn

**Abstract:** In recent years, dynamically tunable structural color has attracted great interest. Here, we introduce the guided-mode resonance (GMR) filter and the phase-change material  $\text{Sb}_2\text{S}_3$  to design a reflective optical metasurface to produce tunable structural color, in which the combination of the GMR filter, with narrow resonant wavelength, and the  $\text{Sb}_2\text{S}_3$ , with a much larger bandgap and higher refractive index, helps to produce high-quality tunable structural color. The simulation results indicate that through the phase transition between the amorphous and crystalline states of  $\text{Sb}_2\text{S}_3$ , the proposed metasurface can generate tunable structural color that can be perceived by the naked eye. Furthermore, the metasurface can sensitively sense environmental changes through changes in structural color. This work provides a new method for realizing dynamically tunable structural color, and paves the way for the application of controllable structural color in dynamic displays, optical stealth, colorimetric sensing, and other fields.

**Keywords:** tunable structural color; guided-mode resonance; phase-change material

## 1. Introduction

Light, which carries a large amount of information, enters the eyes through the pupils, helping people to understand the colorful world. One of the most intuitive manifestations of this information is color. Human beings have studied and applied color for thousands of years. Currently, dyes and pigments still play a leading role in our lives as coloring materials. The common colors in nature are mainly divided into pigment colors and structural colors, according to their production mechanism. The oldest scientific description of structural color is found in *'Micrographia'*, written by Hooke, in 1665 [1]. In the past 30 years, structural color has attracted great attention as a promising alternative to dye- and pigment-based color [2]. Structural color is obtained by the scattering, diffraction, and interference of light from periodic micro-nanostructures [3]. Therefore, it has the advantages of large gamut, high saturation, high-resolution, and environmental friendliness, among others [4]. Halas et al. designed a tunable visible color-changing metasurface, which can be used as both a strain sensor and a localized surface-plasmon-resonance refractive-index sensor, with remarkable color tenability [5]. Lin et al. experimentally demonstrated the refractive-index-sensing property of a metamaterial grating device integrated with a polydimethylsiloxane microfluidic chip. The color changes of the metamaterial grating device induced by the refractive index in an ambient light environment were clear to the naked eye [6]. Based on previous research, we can conclude that structural colors mainly include metal-metasurface structural colors and all-dielectric metasurface structural colors from the perspective of material composition [4–9]. Metal-metasurface structural color has subwavelength resolution but suffers from low intensity and small gamut because of the inherent ohmic loss of metal. All-dielectric metasurface structural color has a high level of brightness, but its resolution is not as high as that of metal metasurfaces. In addition to the optimization of parameters, dynamic adjustment is also one of the key factors in determining the practicality of structural color [10]. With the further development



**Citation:** Luo, S.; Zhang, Z.; He, X.; Zhang, Z.; Li, X.; Fu, M.; Yang, J. Design of Reflective Tunable Structural Color Metasurface Based on Guided-Mode Resonance Filter and  $\text{Sb}_2\text{S}_3$ . *Photonics* **2023**, *10*, 752. <https://doi.org/10.3390/photonics10070752>

Received: 19 May 2023  
Revised: 26 June 2023  
Accepted: 26 June 2023  
Published: 29 June 2023



**Copyright:** © 2023 by the authors. Licensee MDPI, Basel, Switzerland. This article is an open access article distributed under the terms and conditions of the Creative Commons Attribution (CC BY) license (<https://creativecommons.org/licenses/by/4.0/>).

of micro-nano-processing technology, dynamically tunable structural color will become increasingly possible.

One way to achieve tunable structural color is to turn individual elements on or off with predetermined colors. For example, Chen et al. proposed a polarization-sensitive color filter based on a titanium-oxide metasurface and realized hue- and saturation-tuned color [11], but it was difficult to realize the miniaturization of the device with the design strategy proposed. Another way to realize tunable structural color is to directly change the refractive index of the surrounding environment of the metasurface by controlling the state or component of the material. This is an ideal method with which to obtain dynamic structural colors. Duan et al. designed a magnesium-based pixelated Fabry–Pérot cavity to generate tunable color displays [12]. The hydrogenation/dehydrogenation kinetics of magnesium cause dynamic changes in FP resonance, resulting in significant color alterations. However, the color-change process requires a long response time, which affects its practical application. Shang et al. designed a microfluidic reconfigurable metasurface and realized real-time adjustable structural color [13]. However, the manufacturing process is complicated. In the past decade, an increasing number of studies have been performed on the use of phase-change materials (PCMs) in dynamically tunable structural color [14,15]. Due to their narrow bandwidths, GMR filters have great potential for realizing the high saturation of structural color and improving the sensitivity of devices to refractive-index changes. In this study, we attempted to integrate a GMR filter and a phase-change material,  $\text{Sb}_2\text{S}_3$ , into the metasurface to realize dynamically tunable structural color. We present the design of an optical metasurface and the investigation of the optical characteristics of the GMR filter in Section 2. We obtained three primary colors by setting the appropriate structural parameters, and took the red color as an example to investigate dynamically tunable structural color, as reported in Section 3. We found that when  $\text{Sb}_2\text{S}_3$  is in the amorphous state, the chromaticity coordinates are (0.5920, 0.3238) and, when  $\text{Sb}_2\text{S}_3$  is in the crystalline state, the chromaticity coordinates are (0.5692, 0.3809). The linear distance between the two chromaticity coordinates is approximately 0.06. It can be concluded that changing the phase state of the material  $\text{Sb}_2\text{S}_3$  can obtain tunable structural color with noticeable changes that can be perceived by the naked eye, as shown in the CIE 1931 chromaticity diagram. Finally, we defined the sensing sensitivity  $s$  of the metasurface and calculated the maximum and minimum values of the sensing sensitivity  $s$  when the refractive index of the surrounding environment changed by 0.1, according to whether the  $\text{Sb}_2\text{S}_3$  is amorphous or crystalline. The results show that the designed metasurface can sensitively display changes in environmental media, similar to a colorimeter.

## 2. Design of Metasurface

### 2.1. Main Structure

The transition of PCMs between different states can change their refractive indices, thereby altering the optical response characteristics. Hence, we can use this feature of PCMs to realize dynamic tuning of structural color. Based on previous research results, we attempted to use  $\text{Sb}_2\text{S}_3$  in a GMR structure to achieve dynamically tunable structural color. The schematic diagram of tunable structural-color metasurface with the GMR grating is shown in Figure 1. In our designed structure, both the grating layer and waveguide layer are composed of  $\text{Si}_3\text{N}_4$ , and have the same refractive index,  $n_2 = n_3$ . Furthermore,  $p$  is the period of grating,  $h$  denotes the height of grating layer, and  $h_3$ ,  $h_4$ , and  $h_5$  represent the thickness of waveguide layer, substrate, and phase-change material, respectively.

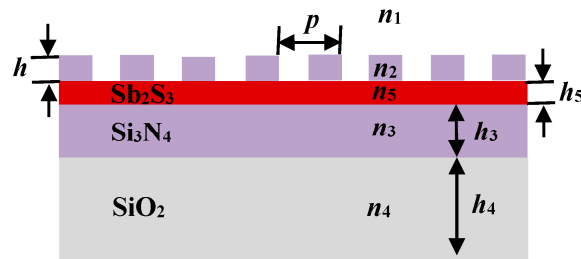


Figure 1. The schematic diagram of reflective tunable-structural-color metasurface.

2.2. Optical Property of GMR Filter

The GMR represents a kind of phenomenon observed in waveguide-grating structures, where the intensity of diffractive field undergoes a rapid variation within small parameter ranges when an incident wave is coupled into a leaky waveguide mode [16,17]. The GMR filter is a unique kind of filter, and the full width half maximum (FWHM) of reflection/transmission spectrum can reach below 5 nm [18–20]. The reflectance of resonance peak is higher than 95%, and the sideband reflectance can be made lower than 5% [18]. Therefore, it is theoretically possible to obtain high-purity filtered light by using a GMR filter. In our work, we attempted to use the metasurface structure containing GMR filter with different parameters to generate the three primary colors. The schematic diagram of the side view (a) and the top view (b) of the optical metasurface obtaining GMR filter is shown in Figure 2. The region  $L_2$  is the grating layer with refractive index  $n_2$ , the region  $L_3$  is the waveguide layer with refractive index  $n_3$ , the cover layer  $L_1$  is the environmental medium with refractive index  $n_1$ , and the lower layer  $L_4$  is the substrate with refractive index  $n_4$ .

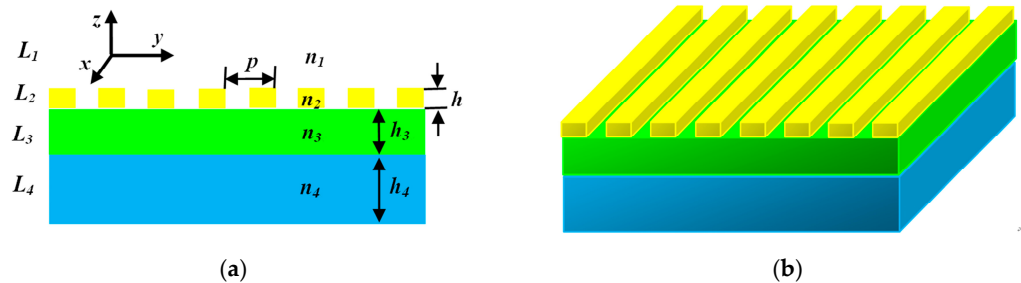


Figure 2. The schematic diagram of the side view (a) and the top view (b) of GMR filter.

When a beam of light is incident on the grating surface, there are two polarization states of the light, which transmits through the one-dimensional (1D) grating. According to [21], the light is transmitted only when the magnetic field,  $H$ , is parallel to the slits. As a consequence, only the incident wave with TM-polarized mode can excite the GMR for 1D grating. When the TM-polarized light in  $y$ - $z$  plane is incident on the grating surface at any angle, the diffraction wave with certain order through the grating resonates with the guided mode of the waveguide layer, provided the refractive indices of the filter material meet the following condition:

$$\max(n_1, n_4) < n_{eff} < n_3, \tag{1}$$

where  $n_{eff} = \sqrt{fn_2^2 + (1-f)n_1^2}$  is the effective refractive index of the grating, and  $f$  is the duty cycle. The coupled wave propagates along the  $y$  direction in the waveguide layer, and it meets the relation as follows [22]:

$$k_y^{(n)} = k_y^{(0)} \pm k_p, \tag{2}$$

where  $k_y^{(0)} = 2\pi n_1 \sin(\theta_i) / \lambda_i$  is the component of the incident wave vector  $k_i$  parallel to the  $x$ - $y$  plane,  $k_p = 2\pi n / p$  is the wave vector regulated by the periodic grating structure,  $k_y^{(n)}$  is the wave vector of  $n$ -order diffraction wave,  $\lambda_i$  is the wavelength in free-space,  $\theta_i$  is the incident angle,  $p$  is the period of the grating, and  $n \geq 1$  is a positive integer representing the diffraction order. When the wave vector of the diffraction wave matches the counterpart of the guided-mode, the resonance occurs and the light field in the waveguide layer is redistributed. As we know, the first-order diffraction wave can excite the strongest resonance. Therefore, we consider the coupling between the first-order diffraction wave and the guided mode, and the resonance wavelength is denoted as  $\lambda_R$ . Using the equation:

$$k_y^{(1)} = 2\pi / \lambda_R = k_y^{(0)} \pm \frac{2\pi}{p}, \tag{3}$$

we can obtain the resonant wavelength  $\lambda_R$ , which is the wavelength of the guided mode propagating in the waveguide layer. From Equation (3), we also know that the wavelength of GMR can be adjusted by changing the grating period  $p$ .

In order to obtain high-quality color with GMR filter, we investigated a large number of previous research results. The investigation found that the materials most frequently used in the grating layer of the GMR structure are  $\text{SiO}_2$  and  $\text{Si}_3\text{N}_4$ , and the materials most frequently used in the waveguide layer are  $\text{Si}_3\text{N}_4$  and  $\text{HfO}_2$ . In our work, in order to facilitate the device preparation, we used the same material,  $\text{Si}_3\text{N}_4$ , in the grating layer and the waveguide layer, as in [23]. Furthermore, we used finite-difference time-domain (FDTD) solutions to analyze the optical property of the GMR filter. A series of reflection spectra were obtained by changing the period  $p$  of the grating in the simulation, as shown in Figure 3. The maximum value of all reflection spectra was above 98%. The FWHM of the reflection spectrum was about 6.5 nm to 8.5 nm, and increased slightly with the red shift of the wave peak. That is to say, when the period  $p$  was 251 nm, the FWHM was 6.5 nm, and when the period  $p$  was 395 nm, the FWHM was 8.5 nm. We also found that when the period  $p$  increased by about 35 nm, the resonance peak shifted red by about 50 nm. Therefore, it can be concluded that the GMR filter has very high reflectivity throughout the visible light band from 400 nm to 700 nm.

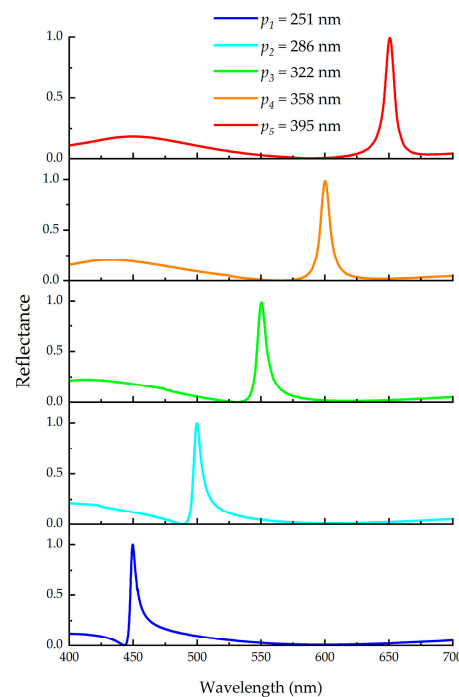


**Figure 3.** The reflection spectra corresponding to different grating period,  $p$ .

From the electric field distributions, we found that the strong electric energy was confined in the waveguide layer. Through further simulation, we found that the incident light was mainly coupled into the metasurface through the ridges of the grating and formed resonance in the waveguide layer. The electric and magnetic field distributions at the resonance wavelength in the GMR filter are shown in Figure 4. The waveguide layer and the ridge of the grating are marked with white dashed lines in the figures, which verify that the GMR occurred and the coupled wave propagated along the  $y$  direction in the waveguide layer. The changes in parameters, such as the grating period  $p$  and the thickness of waveguide layer  $h_3$ , had a significant impact on GMR.

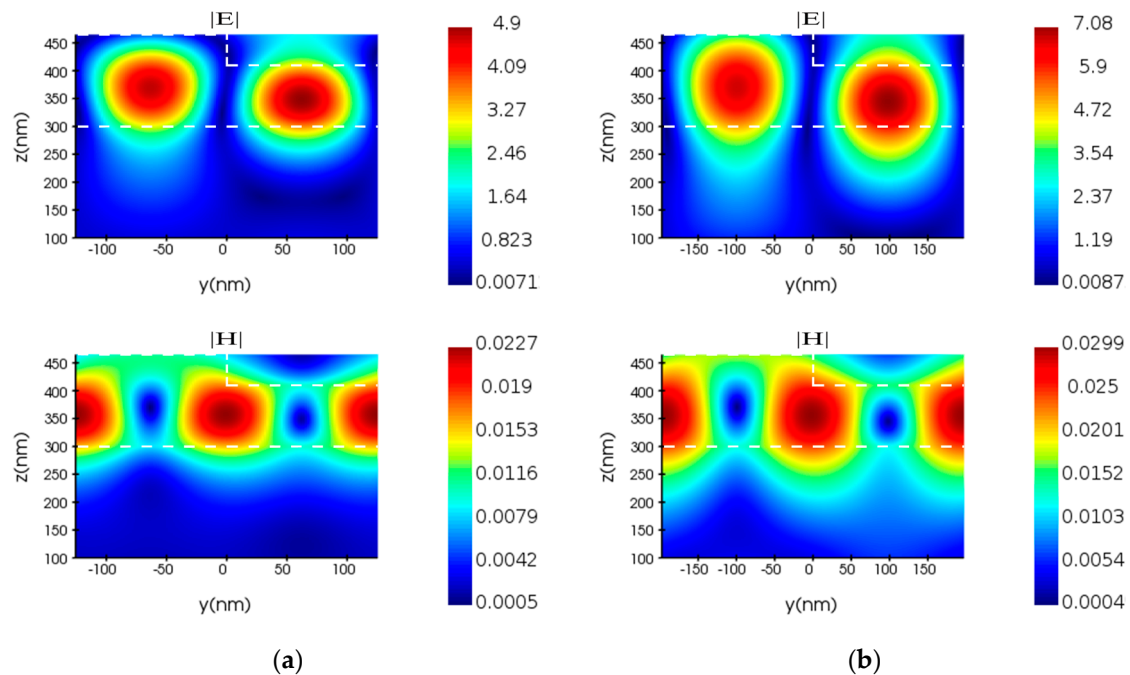


**Figure 4.** The electric and magnetic field distribution maps in GMR filter correspond to the grating periods (a)  $p = 251$  nm and (b)  $p = 395$  nm, respectively.

### 2.3. Optical Properties of $Sb_2S_3$

The use of PCMs has attracted significant interest from scholars researching structural color because of its unique optical properties [24]. Optical or electrical pulses and mechanical stress can be utilized to switch materials between amorphous and crystalline states, so as to make the refractive index of PCMs change sharply and obtain a different ability to confine the light field. Common PCMs include GeTe,  $Ge_2Sb_2Te_5$  (GST),  $Ge_2Sb_2Se_4Te_1$  (GSST),  $VO_2$ , and  $TiO_2$ , etc. [25–28]. The phase-state switching of GST is non-volatile in nature, while the phase transition of  $VO_2$  is volatile [29]. Compared with materials that require a constant energy supply to maintain their phase and optical properties, non-volatile PCMs are more attractive for practical applications [30].

Furthermore,  $Sb_2S_3$  is an unconventional phase-change material, which has a much larger bandgap and, concomitantly, lower absorption. Its higher refractive index and low phonon frequency make it attractive for applications that require high transmission from the visible to the mid-infrared [30,31]. According to [31], we know the refractive indices of  $Sb_2S_3$  in the visible-light band, as shown in Figure 5. Here, a $Sb_2S_3$  represents  $Sb_2S_3$  in the amorphous state and c $Sb_2S_3$  represents  $Sb_2S_3$  in the crystalline state.

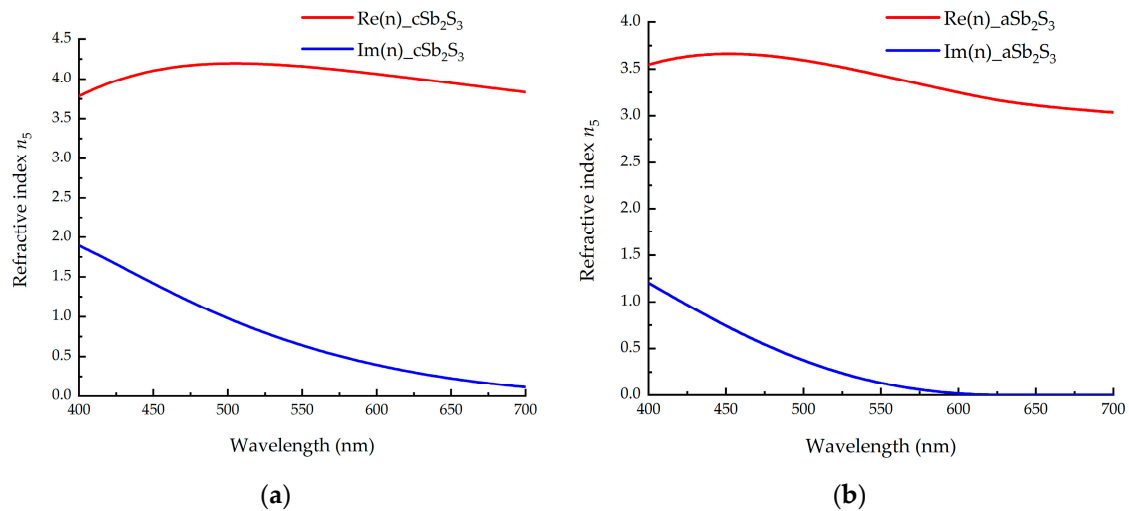


**Figure 5.** The refractive-index distribution of  $\text{Sb}_2\text{S}_3$  in (a) crystalline and (b) amorphous states in visible-light band. The red line represents the real part of the refractive index  $n_5$ , and the blue line represents the imaginary part of the refractive index  $n_5$ .

We can see that the real part of the refractive index of  $\text{Sb}_2\text{S}_3$  is relatively large in the visible light band, and it has a strong ability to confine light. At the same time, the imaginary part of its refractive index is small, indicating that the absorption of light is very weak. In fact, in the visible-light band, the extinction coefficient of  $\text{Sb}_2\text{S}_3$  is much smaller than that of the GST, and the real part of the refractive index of the  $\text{Sb}_2\text{S}_3$  is larger than that of the GST in the crystalline state [30]. Compared with the GST and  $\text{VO}_2$ , the refractive index of  $\text{Sb}_2\text{S}_3$  varies greatly during the structural-phase transition in the visible range [32]. Therefore,  $\text{Sb}_2\text{S}_3$  is well suited to tunable active photonics.

### 3. Simulations of Dynamically Tunable Structural Color

#### 3.1. Structural Color Characteristics of the Designed Metasurface

Herein, we mainly study the characteristics of the wave reflected from the metasurface in Figure 1. The thickness of the substrate silica is relatively large. In our simulation, the thickness  $h_4$  of the substrate was always greater than 200 nm. After many simulations, the optimal thickness  $h_5$  of  $\text{Sb}_2\text{S}_3$  was 10 nm, and the optimum value of the grating-duty cycle was 0.5. On the basis of these results, we further studies the optical properties of the designed metasurface by changing one of the parameters  $h$ ,  $p$ , and  $h_3$ . We used FDTD solutions to sweep one of the three parameters while keeping the other two unchanged. When  $p = 360$  nm,  $h = 70$  nm, and  $h_3 = 80$  nm, the best red color was obtained. The reflection spectrum and the CIE 1931 chromaticity diagram are shown in Figure 6, which contains the results of three different grating heights. When  $h$  was adjusted, the reflectivity at the resonance wavelength changed little, but the sidebands on both sides changed significantly. During the simulation, we found that the influence of the thickness of the phase-change material  $\text{Sb}_2\text{S}_3$  on the position of the resonant peak was greater than that of the waveguide layer. Next, we obtained the best green color when  $p = 290$  nm,  $h = 70$  nm, and  $h_3 = 80$  nm. The corresponding reflection spectrum and the chromaticity diagram are shown in Figure 7, which contains the results of three different grating periods. As the period  $p$  increased, the resonance peak shifts red and the reflectivity also increased. Finally, we obtained the best blue color when  $p = 260$  nm,  $h = 100$  nm, and  $h_3 = 60$  nm. The corresponding reflection spectrum and the chromaticity diagram are shown in Figure 8, which contains the results of three different thicknesses of the waveguide layer.

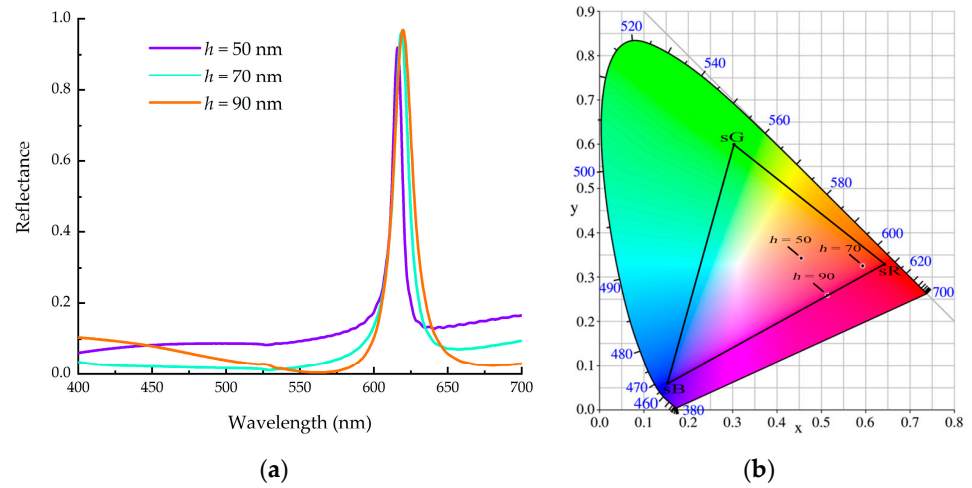


**Figure 6.** (a) the reflection spectrum and (b) the CIE 1931 chromaticity diagram corresponding to red color.

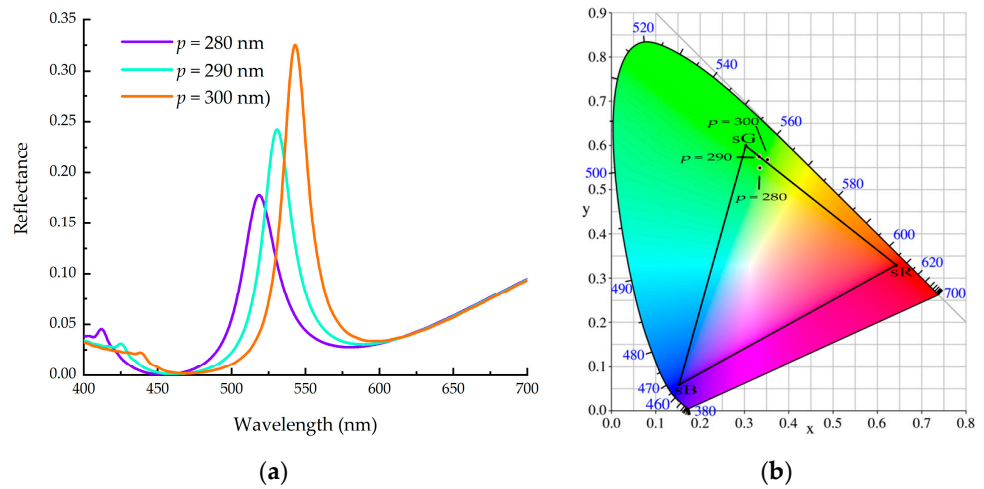


**Figure 7.** (a) the reflection spectrum and (b) the CIE 1931 chromaticity diagram corresponding to green color.

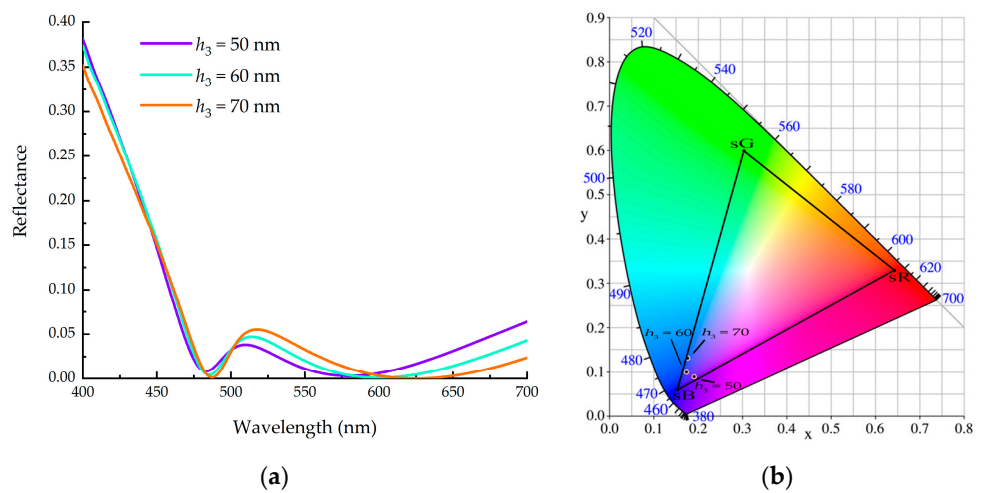


**Figure 8.** (a) the reflection spectrum and (b) the CIE 1931 chromaticity diagram corresponding to blue color.

From the simulation results, we found that the efficiency of the generation of green and blue colors by using the proposed metasurface structure was relatively low. This was mainly caused by the optical properties of the phase-change material itself, as the  $\text{Sb}_2\text{S}_3$  had relatively large extinction coefficients in the green and blue bands. The results in Figure 3 indicate that the GMR filter can efficiently generate three primary colors. However, from the results in Figures 7 and 8, it can be seen that the combination of the GMR filter and PCMs was not yet perfect. This is a further problem that we need to strive to solve by, for example, searching for materials with lower extinction coefficients in the green and blue bands to replace  $\text{Sb}_2\text{S}_3$ . After preliminary investigation,  $\text{In}_2\text{Se}_3$  was found to be a possible candidate material, which is expected to generate both green and blue colors more efficiently.

### 3.2. Dynamic Tuning Characteristics

As shown in Section 2.3, we found that the refractive index of the phase-change material,  $\text{Sb}_2\text{S}_3$ , underwent a significant change as it transitioned from the amorphous to the crystalline state. In this section, we take the red band as an example to study the color-dynamic-tuning ability of the designed optical metasurface. Firstly, we simulated a case in which the  $\text{Sb}_2\text{S}_3$  was in the amorphous state. The heights  $h$  of the grating were set to 60 nm, 70 nm, and 80 nm, respectively. The period  $p$  was set to 350 nm, 360 nm, and 370 nm, respectively. Secondly, we simulated a case in which the  $\text{Sb}_2\text{S}_3$  was in the crystalline state. The values of the parameters  $h$  and  $p$  were the same as those in the amorphous state. The simulated results are shown in Figure 9. Compared with the simulation results, it was found that when the  $\text{Sb}_2\text{S}_3$  was amorphous, the metasurface had a higher reflectivity, as shown in Figure 9a,c,e, and the obtained structural-color brightness is better. This was related to the low extinction coefficient of the amorphous  $\text{Sb}_2\text{S}_3$ . Additionally, it can be seen from the chromaticity diagram that when the  $\text{Sb}_2\text{S}_3$  was amorphous, changing the height  $h$  or period  $p$  of the grating resulted in a more obvious change in the obtained structural color, as shown in Figure 9b,d,f. In these three figures, the  $ap$  and  $cp$  represent the parameters of period  $p$  when the  $\text{Sb}_2\text{S}_3$  was in the amorphous and crystalline states, respectively. The figures show that the designed metasurface structure was more sensitive when the  $\text{Sb}_2\text{S}_3$  was amorphous. From the reflection spectrum, we also found that the resonance wavelength shifted red with the increase in the grating period  $p$ . This was consistent with the theoretical prediction given by Equation (3). From the color palettes in Figure 9g, we found that when changing the phase state of the  $\text{Sb}_2\text{S}_3$ , significant color changes were observed in the metasurface structure, even with different parameters. In Figure 9g, the horizontal axis represents the height  $h$  of the grating and the phase state of the  $\text{Sb}_2\text{S}_3$ , and the vertical axis represents the period  $p$  of the grating. For example, the three color blocks in the first column, from the bottom to the top, correspond to the colors where  $\text{Sb}_2\text{S}_3$  is in an amorphous state, the grating height  $h$  is 60 nm, and the grating periods  $p$  are 350 nm, 360 nm, and 370 nm, respectively.

We can transform  $\text{Sb}_2\text{S}_3$  from the amorphous to the crystalline state by heating the material. Using electrical or optical pulses with tunable pulse length and power can reversibly crystallize and amorphize  $\text{Sb}_2\text{S}_3$ . Compared to optical switching excitation, electrical switching excitation has more advantages because it does not require complex alignment processes. Fang et al. found that the material  $\text{Sb}_2\text{S}_3$  started to crystallize at  $\approx 523$  K, and the grain growth reached completion at 573 K [33]. Muskens et al. found that the transition temperature of  $\text{Sb}_2\text{S}_3$  is 543 K [31]. By heating the material above its melting temperature and then quenching the sample faster than the crystallization speed, we can also change  $\text{Sb}_2\text{S}_3$  from the crystalline to the amorphous state [31,33]. The material  $\text{Sb}_2\text{S}_3$  can be switched between amorphous and crystalline states on a nanosecond time scale, and the switching time is about 78 ns [30]. Mei et al. confirmed through experiments that the cycling durability that  $\text{Sb}_2\text{S}_3$  can achieve is 7000 cycles [34].

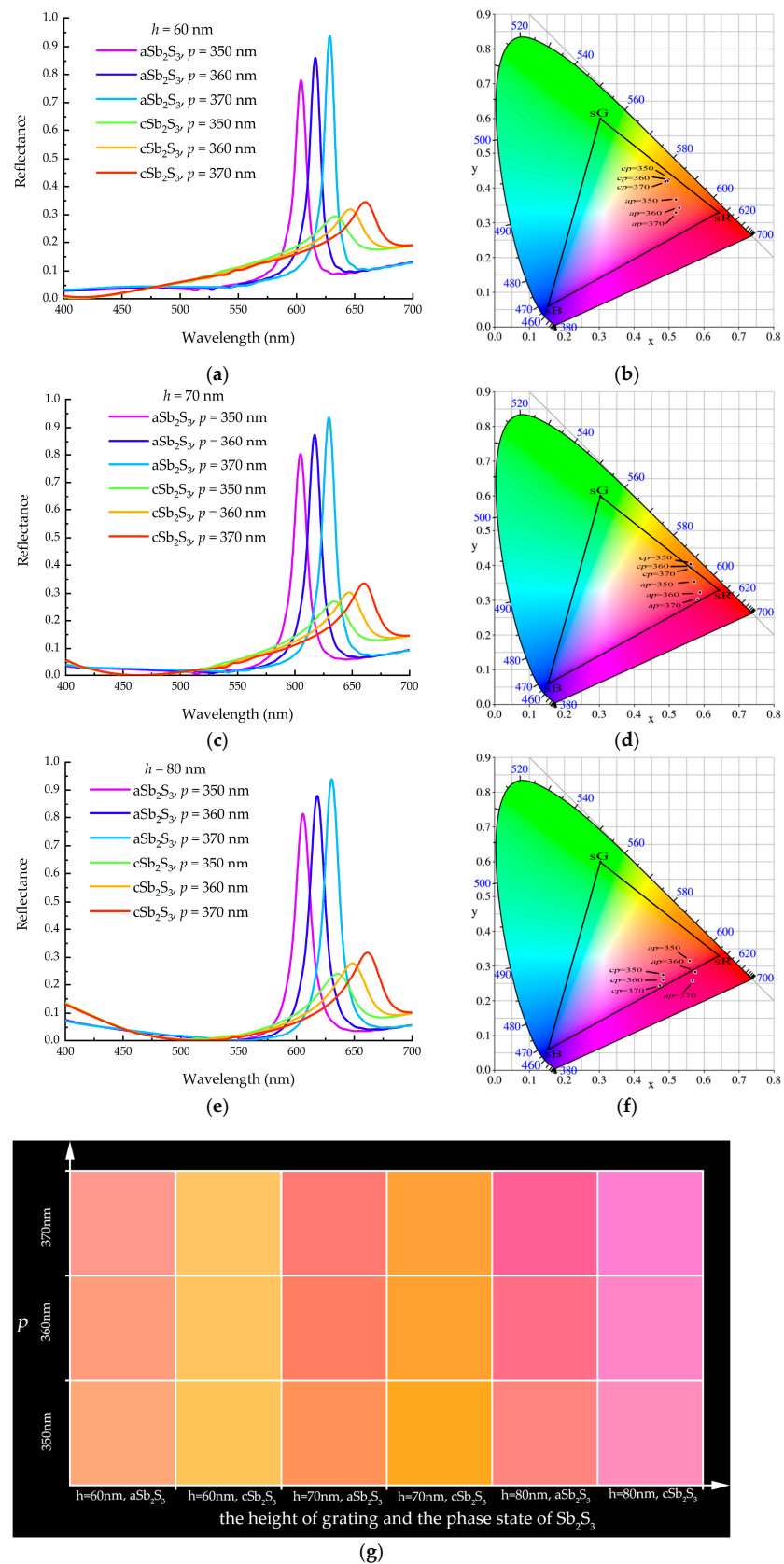


**Figure 9.** The tunable structural color obtained from the designed metasurface with  $\text{Sb}_2\text{S}_3$  in amorphous and crystalline states: (a,c,e) are the reflection spectra corresponding to  $h = 60$  nm,  $70$  nm,  $80$  nm, respectively; (b,d,f) are the chromaticity diagrams corresponding to  $h = 60$  nm,  $70$  nm,  $80$  nm, respectively; (g) is the color palettes corresponding to these reflection spectra.

Compared to materials such as GST, GSST, and VO<sub>2</sub>, Sb<sub>2</sub>S<sub>3</sub> has a larger band gap [33,35–37], resulting in lower light absorption and, thus, greater structural color brightness. The phase-change temperature of Sb<sub>2</sub>S<sub>3</sub> is higher than those of GST and VO<sub>2</sub> [14,31] and lower than that of GSST [31], indicating that Sb<sub>2</sub>S<sub>3</sub> is not be the best choice if energy consumption is the primary consideration. The crystallization switching time of Sb<sub>2</sub>S<sub>3</sub> is 78 ns, which is equivalent to that of GST and better than that of GSST [26,38]. The switching time of VO<sub>2</sub> between the metal and the semiconductor is about 2~3 ns in an electrically driven manner [39]. In short, the switching time of Sb<sub>2</sub>S<sub>3</sub> is sufficient in terms of practicality. The cycling endurance of GST and GSST is about 10<sup>5</sup> cycles [25,40], which is far better than that of Sb<sub>2</sub>S<sub>3</sub>. Of course, with the progress of technology and the improvement of heating methods, the cycling durability of Sb<sub>2</sub>S<sub>3</sub> will be further improved. The main parameters of the four PCMs mentioned above are shown in Table 1.

**Table 1.** Comparison between main parameters of Sb<sub>2</sub>S<sub>3</sub> and those of other common PCMs.

PCMs	Bandgap	Transition Temperature	Switching Time	Drive Manner	Cycling Durability	Phase-Change Property	Ability to Tune Color
Sb <sub>2</sub> S <sub>3</sub>	1.7~2 eV [33]	270 °C/543 K [31]	78 ns [30]	light-operated, 45~55 mw [31]	>7000 cycles [34]	non-volatile	high
GST	0.5~0.7 eV [35]	160 °C/433 K [14]	50 ns [26]	electric control, 1.2 V [41]	>10 <sup>15</sup> cycles [25]	non-volatile	low
GSST	0.42~0.73 eV [36]	400 °C/673 K [31]	300 ns [38]	electric control, <12 V [40], 5~24 V [42]	10 <sup>5</sup> cycles [40]	non-volatile	medium
VO <sub>2</sub>	0.6 eV [37]	68 °C/341 K [31]	2~3 ns [39]	electric control 20.68 V [43]		volatile	medium

In general, the higher the refractive index of a material, the stronger its ability to localize light. The greater the change in refractive index of PCMs during the phase-change process, the stronger their ability to tune structural color. The smaller the extinction coefficient of a material, the less light it absorbs, and the resulting structural color brightness is higher. Based on these principles, we analyzed the ability of these four PCMs to tune structural color by comparing their refractive index, extinction coefficient, and refractive-index-variation values. In contrast, Sb<sub>2</sub>S<sub>3</sub> has a higher ability to tune structural color.

### 3.3. Environment-Sensing Properties of Tunable Structural Color Metasurface

In this section, we report the simulation of an application scenario in which the designed metasurface was used to characterize the change of the refractive index  $n_1$  of the cover layer. When the Sb<sub>2</sub>S<sub>3</sub> remained in the amorphous or crystalline state, we swept the refractive index  $n_1$  from 1 to 1.5 in steps of 0.1. The obtained chromaticity diagrams and color palettes are shown in Figure 10. When Sb<sub>2</sub>S<sub>3</sub> was in the amorphous state and the refractive index  $n_1$  changed from 1 to 1.5, the chromaticity coordinates were (0.5920, 0.3238), (0.6088, 0.3232), (0.5759, 0.2899), (0.4687, 0.2150), (0.4131, 0.1992), and (0.3842, 0.2198), respectively. Additionally, when the refractive index  $n_1$  changed by 0.1, the minimum linear distance between the chromaticity coordinates before and after the refractive index change was about 0.017, and the maximum linear distance was about 0.131. When the Sb<sub>2</sub>S<sub>3</sub> was in the crystalline state and the refractive index  $n_1$  changed from 1 to 1.5, the chromaticity coordinates were (0.5692, 0.3809), (0.5727, 0.3949), (0.5047, 0.3516), (0.3759, 0.2433), (0.3286, 0.2265), and (0.3107, 0.2544), respectively. Furthermore, when the refractive index  $n_1$  changed by 0.1, the minimum linear distance between the chromaticity coordinates before and after the refractive index change was about 0.014, and the maximum linear distance was about 0.168. We define the sensing sensitivity  $s$  of the metasurface, and the equation for  $s$  is as follows:

$$s = \Delta d / \Delta n, \tag{4}$$

where  $\Delta n$  is the change in the refractive index of the environmental medium, and  $\Delta d$  is the linear distance between the chromaticity coordinates caused by  $\Delta n$ . According to

Equation (4), when  $Sb_2S_3$  is in the amorphous state and the refractive index  $n_1$  changes by 0.1, the maximum sensing sensitivity  $s$  of the designed metasurface is 1.31, and the minimum value of the sensing sensitivity  $s$  is 0.17. When  $Sb_2S_3$  is in the crystalline state and the refractive index  $n_1$  changes by 0.1, the maximum sensing sensitivity  $s$  of the designed metasurface is 1.68, and the minimum value of sensing sensitivity  $s$  is 0.14.

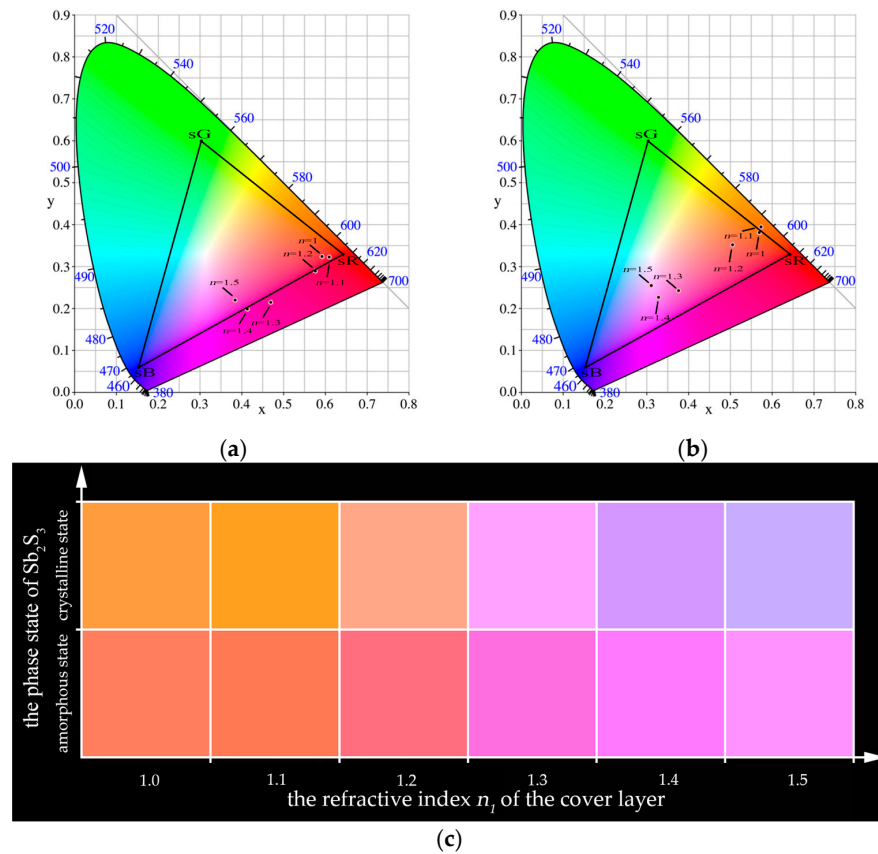


**Figure 10.** The chromaticity diagrams and color palettes with different refractive indices and phase states: (a) chromaticity diagram when  $Sb_2S_3$  is in amorphous state; (b) chromaticity diagram when  $Sb_2S_3$  is in crystalline state; (c) color palettes corresponding to different refractive indices of the cover layer and different phase states of  $Sb_2S_3$ .

On the other hand, when the refractive index  $n_1$  remains constant between 1~1.5, the minimum linear distance between the chromaticity coordinates before and after the phase transition of  $Sb_2S_3$  is 0.061, and the maximum linear distance is 0.097. These results show that the designed metasurface is sensitive to small changes in the refractive index of the cover layer. We can conclude that the metasurface with the phase-change material  $Sb_2S_3$  can sensitively display changes in ambient temperature, humidity, or material composition through color. This is very useful in instruments such as colorimeters.

**4. Conclusions**

In summary, we investigated the optical properties of a GMR filter and the phase-change characteristic of the material  $Sb_2S_3$ , and introduced a GMR filter and  $Sb_2S_3$  into the optical metasurface to produce tunable structural color. The simulation results show that dynamically tunable structural color can be obtained through the phase transition of  $Sb_2S_3$  between the amorphous and crystalline states. Taking the red color as an example, when  $Sb_2S_3$  changes from the amorphous to the crystalline state, the chromaticity coordinate changes from (0.5920, 0.3238) to (0.5692, 0.3809). The linear distance between two chromaticity coordinates is about 0.06. Finally, we applied the designed optical metasurface to check the refractive-index changes caused by changes in ambient temperature, humidity, or

material composition. It can be concluded that the metasurface we proposed can sensitively sense changes in the environment. This work provides a new idea for realizing dynamically tunable structural color, and paves the way for the application of controllable structural color in dynamic displays, optical stealth, colorimetric sensing, and other fields. We believe that dynamically controllable structural color will increasingly enter individuals' lives with the further development of nano-processing technology.

**Author Contributions:** Conceptualization, S.L.; methodology, X.H.; software, Z.Z. (Zhaojian Zhang); data curation, S.L. and X.L.; writing—original draft preparation, S.L.; writing—review and editing, Z.Z. (Zhaojian Zhang) and J.Y.; visualization, S.L.; supervision, M.F. and J.Y.; project administration, Z.Z. (Zhenfu Zhang) and J.Y. All authors have read and agreed to the published version of the manuscript.

**Funding:** This research was funded by the National Natural Science Foundation of China (60907003, 61805278, 12272407, 62275269, 62275271); National Key R&D Program of China (2022YFF0706005); China Postdoctoral Science Foundation (2018M633704); Foundation of NUDT (JC13-02-13, ZK17-03-01); Hunan Provincial Natural Science Foundation of China (13JJ3001); and Program for New Century Excellent Talents in University (NCET-12-0142).

**Institutional Review Board Statement:** Not applicable.

**Informed Consent Statement:** Not applicable.

**Data Availability Statement:** Not applicable.

**Conflicts of Interest:** The authors declare no conflict of interest.

## References

1. Kinoshita, S.; Yoshioka, S.; Miyazaki, J. Physics of structural colors. *Rep. Prog. Phys.* **2008**, *71*, 076401. [[CrossRef](#)]
2. Baek, K.; Kim, Y.; Mohd-Noor, S.; Hyun, J.K. Mie Resonant Structural Colors. *ACS Appl. Mater. Interfaces* **2020**, *12*, 5300–5318. [[CrossRef](#)] [[PubMed](#)]
3. Nagasaki, Y.; Suzuki, M.; Takahara, J. All-Dielectric Dual-Color Pixel with Subwavelength Resolution. *Nano Lett.* **2017**, *17*, 7500–7506. [[CrossRef](#)]
4. Yang, W.; Xiao, S.; Song, Q.; Liu, Y.; Wu, Y.; Wang, S.; Yu, J.; Han, J.; Tsai, D.-P. All-dielectric metasurface for high-performance structural color. *Nat. Commun.* **2020**, *11*, 1864. [[CrossRef](#)]
5. Cerjan, B.; Gerislioglu, B.; Link, S.; Nordlander, P.; Halas, N.J.; Griep, M. Towards scalable plasmonic Fano-resonant metasurfaces for colorimetric sensing. *Nanotechnology* **2022**, *33*, 405201. [[CrossRef](#)]
6. Zheng, D.Y.; Wen, Y.; Xu, X.C.; Lin, Y.S. Metamaterial grating for colorimetric chemical sensing applications. *Mater. Today Phys.* **2023**, *33*, 101056. [[CrossRef](#)]
7. Tan, S.J.; Zhang, L.; Zhu, D.; Goh, X.M.; Wang, Y.M.; Kumar, K.; Qiu, C.W.; Yang, J.K.W. Plasmonic Color Palettes for Photorealistic Printing with Aluminum Nanostructures. *Nano Lett.* **2014**, *14*, 4023–4029. [[CrossRef](#)] [[PubMed](#)]
8. Zhu, X.L.; Vannahme, C.; Hojlund-Nielsen, E.; Mortensen, N.A.; Kristensen, A. Plasmonic colour laser printing. *Nat. Nanotechnol.* **2016**, *11*, 325–329. [[CrossRef](#)]
9. Sun, S.; Zhou, Z.X.; Zhang, C.; Gao, Y.S.; Duan, Z.H.; Xiao, S.M.; Song, Q.H. All-Dielectric Full-Color Printing with TiO<sub>2</sub> Metasurfaces. *ACS Nano* **2017**, *11*, 4445–4452. [[CrossRef](#)] [[PubMed](#)]
10. Shao, L.; Zhuo, X.L.; Wang, J.F. Advanced Plasmonic Materials for Dynamic Color Display. *Adv. Mater.* **2018**, *30*, 1704338. [[CrossRef](#)] [[PubMed](#)]
11. Yang, B.; Liu, W.W.; Li, Z.C.; Cheng, H.; Chen, S.Q.; Tian, J.G. Polarization-Sensitive Structural Colors with Hue-and-Saturation Tuning Based on All-Dielectric Nanopixels. *Adv. Opt. Mater.* **2018**, *6*, 1701009. [[CrossRef](#)]
12. Chen, Y.Q.; Duan, X.Y.; Matuschek, M.; Zhou, Y.M.; Neubrech, F.; Duan, H.G.; Liu, N. Dynamic Color Displays Using Stepwise Cavity Resonators. *Nano Lett.* **2017**, *17*, 5555–5560. [[CrossRef](#)]
13. Sun, S.; Yang, W.H.; Zhang, C.; Jing, J.X.; Gao, Y.S.; Yu, X.Y.; Song, Q.H.; Xiao, S.M. Real-Time Tunable Colors from Microfluidic Reconfigurable All-Dielectric Metasurfaces. *ACS Nano* **2018**, *12*, 2151–2159. [[CrossRef](#)] [[PubMed](#)]
14. Raeis-Hosseini, N.; Rho, J. Metasurfaces Based on Phase-Change Material as a Reconfigurable Platform for Multifunctional Devices. *Materials* **2017**, *10*, 1046. [[CrossRef](#)] [[PubMed](#)]
15. Schlich, F.F.; Zalden, P.; Lindenberg, A.M.; Spolenak, R. Color Switching with Enhanced Optical Contrast in Ultrathin Phase-Change Materials and Semiconductors Induced by Femtosecond Laser Pulses. *Acs Photonics* **2015**, *2*, 178–182. [[CrossRef](#)]
16. Liu, W.; Lai, Z.; Guo, H.; Liu, Y. Guided-mode resonance filters with shallow grating. *Opt. Lett.* **2010**, *35*, 865–867. [[CrossRef](#)]
17. Priambodo, P.S.; Maldonado, T.A.; Magnusson, R. Fabrication and characterization of high-quality waveguide-mode resonant optical filters. *Appl. Phys. Lett.* **2003**, *83*, 3248–3250. [[CrossRef](#)]

18. Tibuleac, S.; Magnusson, R. Reflection and transmission guided-mode resonance filters. *J. Opt. Soc. Am. A Opt. Image Sci. Vis.* **1997**, *14*, 1617–1626. [[CrossRef](#)]
19. Zhang, S.; Wang, Y.; Wang, S.; Zheng, W. Wavelength-tunable perfect absorber based on guided-mode resonances. *Appl. Opt.* **2016**, *55*, 3176–3181. [[CrossRef](#)]
20. Wang, Q.; Zhang, D.; Xu, B.; Huang, Y.; Tao, C.; Wang, C.; Li, B.; Ni, Z.; Zhuang, S. Colored image produced with guided-mode resonance filter array. *Opt. Lett.* **2011**, *36*, 4698–4700. [[CrossRef](#)]
21. Sakat, E.; Vincent, G.; Ghenuche, P.; Bardou, N.; Dupuis, C.; Collin, S.; Pardo, F.; Haidar, R.; Pelouard, J.L. Free-standing guided-mode resonance band-pass filters: From 1D to 2D structures. *Opt. Express* **2012**, *20*, 13082–13090. [[CrossRef](#)] [[PubMed](#)]
22. Collin, S.; Pardo, F.; Teissier, R.; Pelouard, J.L. Strong discontinuities in the complex photonic band structure of transmission metallic gratings. *Phys. Rev. B* **2001**, *63*, 033107. [[CrossRef](#)]
23. Uddin, M.J.; Magnusson, R. Highly efficient color filter array using resonant Si<sub>3</sub>N<sub>4</sub> gratings. *Opt. Express* **2013**, *21*, 12495–12506. [[CrossRef](#)] [[PubMed](#)]
24. Wuttig, M.; Bhaskaran, H.; Taubner, T. Phase-change materials for non-volatile photonic applications. *Nat. Photonics* **2017**, *11*, 465–476. [[CrossRef](#)]
25. Carrillo, S.G.C.; Trimby, L.; Au, Y.Y.; Nagareddy, V.K.; Rodriguez-Hernandez, G.; Hosseini, P.; Ros, C.; Bhaskaran, H.; Wright, C.D. A Nonvolatile Phase-Change Metamaterial Color Display. *Adv. Opt. Mater.* **2019**, *7*, 1801782. [[CrossRef](#)]
26. Simpson, R.E.; Krbal, M.; Fons, P.; Kolobov, A.V.; Tominaga, J.; Uruga, T.; Tanida, H. Toward the Ultimate Limit of Phase Change in Ge<sub>2</sub>Sb<sub>2</sub>Te<sub>5</sub>. *Nano Lett.* **2010**, *10*, 414–419. [[CrossRef](#)]
27. Gerislioglu, B.; Bakan, G.; Ahuja, R.; Adam, J.; Mishra, Y.K.; Ahmadvand, A. The role of Ge<sub>2</sub>Sb<sub>2</sub>Te<sub>5</sub> in enhancing the performance of functional plasmonic devices. *Mater. Today Phys.* **2020**, *12*, 100178. [[CrossRef](#)]
28. Kepič, P.; Ligmajer, F.; Hrtoň, M.; Ren, H.; Menezes, L.d.S.; Maier, S.A.; Šikola, T. Optically Tunable Mie Resonance VO<sub>2</sub> Nanoantennas for Metasurfaces in the Visible. *ACS Photonics* **2021**, *8*, 1048–1057. [[CrossRef](#)]
29. de Galarreta, C.R.; Sinev, I.; Alexeev, A.M.; Trofimov, P.; Ladutenko, K.; Carrillo, S.G.C.; Gemo, E.; Baldycheva, A.; Bertolotti, J.; Wright, C.D. Reconfigurable multilevel control of hybrid all-dielectric phase-change metasurfaces. *Optica* **2020**, *7*, 476–484. [[CrossRef](#)]
30. Dong, W.; Liu, H.; Behera, J.K.; Lu, L.; Ng, R.J.H.; Sreekanth, K.V.; Zhou, X.; Yang, J.K.W.; Simpson, R.E. Wide Bandgap Phase Change Material Tuned Visible Photonics. *Adv. Funct. Mater.* **2019**, *29*, 1806181. [[CrossRef](#)]
31. Delaney, M.; Zeimpekis, I.; Lawson, D.; Hewak, D.W.; Muskens, O.L. A New Family of Ultralow Loss Reversible Phase-Change Materials for Photonic Integrated Circuits: Sb<sub>2</sub>S<sub>3</sub> and Sb<sub>2</sub>Se<sub>3</sub>. *Adv. Funct. Mater.* **2020**, *30*, 2002447. [[CrossRef](#)]
32. Li, H.X.; Zhang, X.; Zhou, F.; Xiao, X.S.; Xu, Y.L.; Zhang, Z.P. Tunable color gamut based a symmetric microcavity governed by Sb<sub>2</sub>S<sub>3</sub>. *Opt. Commun.* **2022**, *508*, 127683. [[CrossRef](#)]
33. Fang, Z.R.; Zheng, J.J.; Saxena, A.; Whitehead, J.; Chen, Y.Y.; Majumdar, A. Non-Volatile Reconfigurable Integrated Photonics Enabled by Broadband Low-Loss Phase Change Material. *Adv. Opt. Mater.* **2021**, *9*, 2002049. [[CrossRef](#)]
34. Gao, K.; Du, K.; Tian, S.M.; Wang, H.; Zhang, L.; Guo, Y.X.; Luo, B.C.; Zhang, W.D.; Mei, T. Intermediate Phase-Change States with Improved Cycling Durability of Sb<sub>2</sub>S<sub>3</sub> by Femtosecond Multi-Pulse Laser Irradiation. *Adv. Funct. Mater.* **2021**, *31*, 2103327. [[CrossRef](#)]
35. Lee, B.S.; Abelson, J.R.; Bishop, S.G.; Kang, D.H.; Cheong, B.K.; Kim, K.B. Investigation of the optical and electronic properties of Ge<sub>2</sub>Sb<sub>2</sub>Te<sub>5</sub> phase change material in its amorphous, cubic, and hexagonal phases. *J. Appl. Phys.* **2005**, *97*, 093509. [[CrossRef](#)]
36. Zhang, H.; Wang, X.; Zhang, W. First-principles investigation of amorphous Ge-Sb-Se-Te optical phase-change materials. *Opt. Mater. Express* **2022**, *12*, 2497–2506. [[CrossRef](#)]
37. Rana, R.S.; Nolte, D.D.; Chudnovski, F.A. Optical bistability from a thermodynamic phase transition in vanadium dioxide. *Opt. Lett.* **1992**, *17*, 1385–1387. [[CrossRef](#)]
38. Wang, H.; Guo, T.; Xue, Y.; Lv, S.; Yao, D.; Zhou, Z.; Song, S.; Song, Z. The phase change memory features high-temperature characteristic based on Ge-Sb-Se-Te alloys. *Mater. Lett.* **2019**, *254*, 182–185. [[CrossRef](#)]
39. Markov, P.; Marvel, R.E.; Conley, H.J.; Miller, K.J.; Haglund, R.F.; Weiss, S.M. Optically Monitored Electrical Switching in VO<sub>2</sub>. *ACS Photonics* **2015**, *2*, 1175–1182. [[CrossRef](#)]
40. Sahoo, D.; Naik, R. GSST phase change materials and its utilization in optoelectronic devices: A review. *Mater. Res. Bull.* **2022**, *148*, 111679. [[CrossRef](#)]
41. Lee, H.C.; Jeong, J.H.; Choi, D.J. Characterization of phase-change behavior of a Ge<sub>2</sub>Sb<sub>2</sub>Te<sub>5</sub> thin film using finely controlled electrical pulses for switching. *Semicond. Sci. Technol.* **2016**, *31*, 095006. [[CrossRef](#)]
42. De Leonardis, F.; Soref, R.; Passaro, V.M.N.; Zhang, Y.F.; Hu, J.J. Broadband Electro-Optical Crossbar Switches Using Low-Loss Ge<sub>2</sub>Sb<sub>2</sub>Se<sub>4</sub>Te<sub>1</sub> Phase Change Material. *J. Light. Technol.* **2019**, *37*, 3183–3191. [[CrossRef](#)]
43. Sun, X.N.; Qu, Z.M.; Yuan, J.H.; Cheng, E.W.; Wang, P.P.; Wang, Q.G. Voltage-induced phase transition of VO<sub>2</sub>@SiO<sub>2</sub> nanoparticles. *Ceram. Int.* **2021**, *47*, 29011–29022. [[CrossRef](#)]

**Disclaimer/Publisher’s Note:** The statements, opinions and data contained in all publications are solely those of the individual author(s) and contributor(s) and not of MDPI and/or the editor(s). MDPI and/or the editor(s) disclaim responsibility for any injury to people or property resulting from any ideas, methods, instructions or products referred to in the content.